A First Look at the Navigation Design and Analysis for the Orion Exploration Mission 2

Chris D'Souza,[*] and Renato Zanetti[†]

ABSTRACT

This paper will detail the navigation and dispersion design and analysis of the first Orion crewed mission. The optical navigation measurement model will be described. The vehicle noise includes the residual acceleration from attitude deadbanding, attitude maneuvers, CO_2 venting, waste-water venting, ammonia sublimator venting and solar radiation pressure. The maneuver execution errors account for the contribution of accelerometer scale-factor on the accuracy of the maneuver execution. Linear covariance techniques are used to obtain the navigation errors and the trajectory dispersions as well as the DV performance. Particular attention will be paid to the accuracy of the delivery at Earth Entry Interface and at the Lunar Flyby.

The Orion Exploration Mission-2 (EM-2) will be the first Orion mission to carry crew and therefore the mission will be subject to high level of scrutiny. The Orion vehicle is thereby required to return the crew safely in the case of loss of communication with the ground. As such, it needs to be able to navigate autonomously, independent of ground-based measurements, utilizing on-board sensors subject to stringent mass/power/volume constraints. Since the vehicle will be carrying optical cameras, the cislunar navigation system is designed to use images obtained from these cameras, in particular planetary limb measurements and therefore presents unique presents challenges.

[*]GN&C Autonomous Flight Systems Engineer, Aeroscience and Flight Mechanics Division, NASA Johnson Space Center EG6, 2101 NASA Parkway, Houston, Texas, 77058. chris.dsouza@nasa.gov
[†]Assistant Professor, The University of Texas at Austin, Austin Texas, 77XXX.

This paper details the navigation design and analysis of the Orion Exploration Mission 2 (EM-2). The characteristics of a Multi-Trans-Lunar-Injection trajectory with an accompanying free-return trajectory present unique GNC challenges that will be addressed in the paper. This is depicted in Figure 1. Whereas the Orion sensor complement includes two star trackers, the chosen star trackers have a very limited field-of-view. As such, they don't lend themselves to cislunar optical navigation, which needs fields-of-view in excess of 20 degrees. A dedicated optical navigation camera is mounted on the same optical platform as the star trackers. The paper will present analysis (and resulting design) that has been performed to understand the performance of the Orion system for EM-2, with particular attention paid to entry flight path angle constraints and the DV performance.
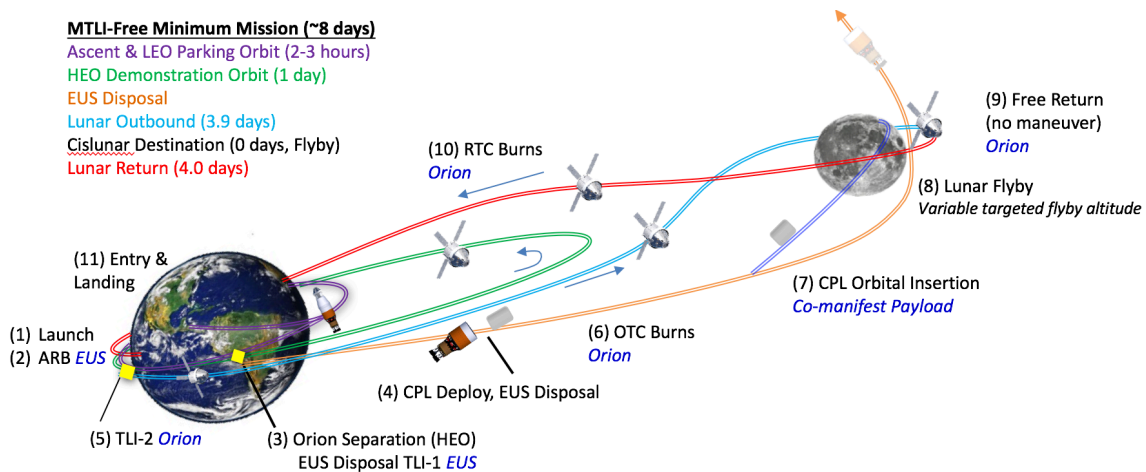
Figure 1. The Orion EM-2 Trajectory Profile

The vehicle noise model includes five sources: attitude deadband residual accelerations, attitude maneuver residual accelerations, pressure swing adsorption (PSA) vents which are used to vent the CO_2 in the crew module, waste water vent accelerations and ammonia sublimator vents. For EM-2 and following, the Pressure Swing Adsorption (PSA) cycles automatically approximately every 10 minutes, less during crew sleep periods, more when the crew is awake – the analysis will also include periods of astronaut exercise each day. The waste water vents are expected to occur every 8 hours. The ammonia sublimator vents are expected to only occur 20 minutes prior to entry. This analysis will assume a 24-jet thruster configuration. Each of the these errors has been

modeled from first-principles and since it is not known *a priori* when these events will occur, they are spread out over the entire mission. The paper will discuss this in detail.

The maneuvers are modeled in terms of scale-factor, bias, misalignment, and noise. Long maneuvers present a particular challenge in meeting accuracy requirements. The accelerometer bias, in particular, is used to model the maneuver scale factor errors which are the major component of maneuver execution error. The paper will discuss this in detail.

The paper will detail the optical camera measurement model used to perform the navigation. The measurements are the planetary centroid and the distance to the planet. This is obtained from the onboard image processing software. The onboard navigation filter then processes these measurements to estimate the inertial position and velocity of the Orion vehicle.

In an emergency situation, during a loss of communication scenario, the primary objective is to secure the safety of the crew. This subsequently translates into a flight-path angle requirement at entry interface (EI) for a direct entry. A direct entry, as opposed to a skip entry, reduces the risk of the capsule bouncing back into space, and allows for a greater margin on the flight-path angle at EI.

Linear covariance analysis will be used to perform the navigation and dispersion analysis for the EM-2 mission. Particular attention will be placed to the trajectory dispersions at the lunar flyby and at entry interface.

The accuracy of the flight-path angle at EI is driven by several factors including the navigation, targeting, and burn execution errors at the time of the last mid-course maneuver, and unaccounted trajectory perturbations between the last mid-course maneuver and EI. Apollo missions tolerated a maximum flight path angle error at EI of ± 1 degree, with half of this error allocated to navigation. A similar criterion is employed in this study. However, for Orion, the EI dispersion error requirement with optical navigation is 0.3 degrees (3σ). The paper will evaluate the accuracy of the delivery in the presence of the aforementioned errors.

LINEAR COVARIANCE ANALYSIS

This investigation is performed using linear covariance (LinCov) analysis techniques.[1,2] The state vector is

$$\mathbf{x} = \left\{ \mathbf{r}^{\mathrm{T}} \quad \mathbf{v}^{\mathrm{T}} \quad \boldsymbol{\theta}^{\mathrm{T}} \quad \mathbf{m}_{op}^{\mathrm{T}} \quad \mathbf{m}_{tr}^{\mathrm{T}} \quad \mathbf{b}_{cent}^{\mathrm{T}} \quad b_{pd} \right\}^{\mathrm{T}}. \tag{1}$$

where $\mathbf{r}$ is the inertial position of the vehicle with respect to the primary body, $\mathbf{v}$ is the corresponding inertial velocity with respect to the primary, $\boldsymbol{\theta}$ is the attitude error, $\mathbf{m}_{op}$ is the misalignment of the optical instrument, $\mathbf{b}_{tr}$ is the bias position of the instrument with respect to the navigation base, $\mathbf{b}_{cent}$ is the bias of the planetary centroid measurement, and b_{pd} is the bias of the planetary diameter measurement.

Neither the attitude error $\delta\boldsymbol{\theta}$ nor its uncertainty are integrated in this analysis. The nominal attitude is known at any time and it does not need to be calculated. The attitude estimation error covariance is treated as a constant and is driven by the star tracker accuracy. The attitude navigation dispersion covariance is also treated as constant and is given by the attitude control dead-band. Before the star elevation is determined, the vehicle slews in preparation for measurement acquisition. This attitude maneuver is performed by the onboard thrusters and is assumed to be instantaneous. Due to thruster misalignment, this maneuver adds uncertainty to the translational states. After the batch of measurements is available, the vehicle returns to its nominal attitude. In linear covariance analysis, the difference between the true state and the nominal state is defined as the environment dispersion

$$\delta\mathbf{x} \triangleq \mathbf{x} - \bar{\mathbf{x}}. \tag{2}$$

The difference between the estimated state and the nominal state is defined as the navigation dispersion

$$\delta\hat{\mathbf{x}} \triangleq \hat{\mathbf{x}} - \bar{\mathbf{x}}. \tag{3}$$

Finally, the difference between the true state and the estimated state, is defined as the estimation

error, sometimes referred to as the onboard navigation error

$$\mathbf{e} \triangleq \mathbf{x} - \hat{\mathbf{x}}. \tag{4}$$

Following the standard Kalman filter assumptions, the difference between the nominal and esti-
mated models is represented with zero-mean, white noise. The estimated state evolves as

$$\dot{\hat{\mathbf{x}}} = \mathbf{f}(\hat{\mathbf{x}}), \tag{5}$$

where $\mathbf{f}$ is a nonlinear function representing the system dynamics as modeled by the filter. The
evolution of the nominal state is modeled as

$$\dot{\bar{\mathbf{x}}} = \bar{\mathbf{f}}(\bar{\mathbf{x}}) = \mathbf{f}(\bar{\mathbf{x}}) + \boldsymbol{v}, \tag{6}$$

where $\bar{\mathbf{f}}$ is a nonlinear function representing the state dynamics as modeled in designing the nom-
inal trajectory. The nominal dynamics $\bar{\mathbf{f}}$ may be higher fidelity than the filter's dynamics $\mathbf{f}$. The
vector $\boldsymbol{v}$ represents the dynamics modeled in the nominal trajectory but neglected in the filter mod-
els. In Kalman filtering, the difference between the true dynamics and the filter's dynamics is called
process noise. While these unmodeled dynamics are not actually white noise, they are modeled as
such. The power spectral density of process noise is then tuned to achieve good performance. The
same procedure is used here. In order to capture the difference between the two dynamical models,
$\boldsymbol{v}$ is modeled as a zero-mean white noise process with power spectral density $\hat{\mathbf{Q}}$. The goal is to
represent the increased value of the navigation dispersion during propagation due to the difference
between the nominal and filter's dynamical models.

The evolution of the navigation dispersion can be approximated to first-order as

$$\delta\dot{\hat{\mathbf{x}}} = \dot{\hat{\mathbf{x}}} - \dot{\bar{\mathbf{x}}} = \mathbf{f}(\bar{\mathbf{x}} + \delta\hat{\mathbf{x}}) - \mathbf{f}(\bar{\mathbf{x}}) - \boldsymbol{v} \simeq \mathbf{F}(\bar{\mathbf{x}})\delta\hat{\mathbf{x}} - \boldsymbol{v}. \tag{7}$$

The evolution of the navigation dispersion covariance is governed by

$$\dot{\hat{P}} = F(\bar{x})\hat{P} + \hat{P}F(\bar{x})^T + \hat{Q}. \tag{8}$$

Similarly, the true state is modeled to evolve as

$$\dot{x} = f(x) + \nu. \tag{9}$$

The evolution of the estimation error is given by

$$\dot{e} = \dot{x} - \dot{\hat{x}} \simeq f(\bar{x}) + F(\bar{x})(x - \bar{x}) + \nu - f(\bar{x}) - F(\bar{x})(\hat{x} - \bar{x}) = F(\bar{x})e + \nu. \tag{10}$$

Vector ν is modeled as zero mean white noise with power spectral density Q. The onboard covariance P evolves as

$$\dot{P} = F(\bar{x})P + PF(\bar{x}) + Q. \tag{11}$$

Notice that the Jacobian F could be evaluated at the estimated state $\hat{x}$ instead of the nominal state $\bar{x}$, as in the extended Kalman filter.

Finally

$$\delta\dot{x} = \dot{x} - \dot{\bar{x}} \simeq F(\bar{x})\delta x + \nu - \upsilon \tag{12}$$

and $\bar{P}$ evolves as

$$\dot{\bar{P}} = F(\bar{x})\bar{P} + \bar{P}F(\bar{x}) + \bar{Q}. \tag{13}$$

Notice that $\bar{Q} = Q + \hat{Q}$ if ν and υ are assumed to be uncorrelated.

OPTICAL NAVIGATION MODEL

Begin with the equations

$$y_h = \tan \alpha_h + b_h + \eta_h = x/z + b_h + \eta_h \qquad (14)$$

$$y_v = \tan \alpha_v + b_v + \eta_v = y/z + b_v + \eta_v \qquad (15)$$

$$\rho = \sqrt{x^2 + y^2 + z^2} = ||\mathbf{r}^i_{orion} - \mathbf{r}^i_P|| \qquad (16)$$

The first two, y_h and y_v, are the centroid measurements and the last one is the range, which will be corrupted a bit further in this section by bias and noise to produce a range measurement.

If the planet is perfectly spherical, the range to the planet would be given by

$$\sin \frac{A}{2} = \frac{R_p}{\rho} \qquad (17)$$

where R_p is the planetary radius and A is the angular diameter. The model assumed in this analysis is a pinhole camera model. The equivalent expression at the focal plane is

$$\tan \frac{A}{2} = \frac{n_d}{2fs} \qquad (18)$$

where n_d is the number of pixels that constitute the angular diameter and s is the pixel pitch (in units of pixels per length, assuming square pixels). This is seen in Figure 2. For what follows, we
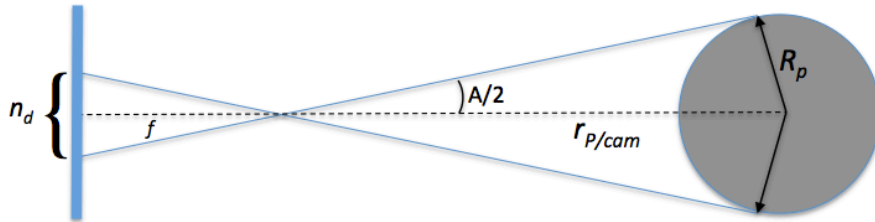
Figure 2. Angular Diameter Measurement

define

$$\delta \;\triangleq\; \frac{n_d}{fs} \tag{19}$$

where δ is a non-dimensional quantity and is the "raw" measurement of the planetary diameter. Consistent with the centroid measurements. Given that the measurements are corrupted with noise, the actual planetary diameter measurement is

$$\tilde{\delta} \;=\; \delta + b_d + \eta_d \;=\; 2\tan\frac{A}{2} + b_d + \eta_d \tag{20}$$

Given that Eq. (18) can be expressed as

$$\tan\frac{A}{2} \;=\; \frac{\delta}{2} \tag{21}$$

using elementary trigonometry, the above equation (Eq. (21)) can be written as

$$\sin\frac{A}{2} \;=\; \frac{\delta}{\sqrt{\delta^2 + 4}} \tag{22}$$

Eq. (17) and Eq. (22) are equated to solve for δ yielding

$$\delta \;=\; \frac{2R_p}{\sqrt{\rho^2 - R_p^2}} \tag{23}$$

or equivalently ρ can be written in terms of δ as

$$\rho \;=\; R_p\sqrt{1 + \left(\frac{2}{\delta}\right)^2} \tag{24}$$

and acknowledging the fact that the measurement is corrupted with noise and bias, we get

$$y_\rho \;=\; R_p\sqrt{1 + \left(\frac{2}{\delta + b_d + \eta_d}\right)^2} \tag{25}$$

8

The Measurement Error Calculations

In LinCov we model the pixel centroid measurements as

$$u = u_p - fs \tan \alpha_h = u_p - fs \, y_h \qquad (26)$$

$$v = u_p - fs \tan \alpha_v = v_p - fs \, y_v \qquad (27)$$

so that

$$du = -(fs)dy_h \qquad (28)$$

$$du = -(fs)dy_h \qquad (29)$$

With this in hand,

$$\sigma_u = (fs)\,\sigma_{y_h} \qquad (30)$$

$$\sigma_v = (fs)\,\sigma_{y_v} \qquad (31)$$

and

$$\sigma_{y_h} = \frac{1}{fs}\sigma_u \qquad (32)$$

$$\sigma_{y_v} = \frac{1}{fs}\sigma_v \qquad (33)$$

We have been assuming in LinCov that the pixel pitch is 4.8×10^{-6} m/pixel and the focal length is 35.1 mm so that

$$\frac{1}{fs} = 1.3675 \times 10^{-4}\,\text{pixels}^{-1} \qquad (34)$$

9

which is equivalent to 28.2 arc-seconds per pixel ($= 1.3675 \times 10^{-4} \cdot 3600 \cdot 180/\pi$) and

$$\sigma_u = 0.06 + \frac{2.12 \times 10^{12}}{\rho^{3/2}} \text{ pixels} \tag{35}$$

$$\sigma_v = 0.06 + \frac{2.12 \times 10^{12}}{\rho^{3/2}} \text{ pixels} \tag{36}$$

where ρ is the distance of the vehicle with respect to the planet (in ft).

Therefore, the required accuracy on the two centroid 'tangent angles' is

$$\sigma_{y_h} = 8.205 \times 10^{-6} + \frac{2.899 \times 10^8}{\rho^{3/2}} \tag{37}$$

$$\sigma_{y_v} = 8.205 \times 10^{-6} + \frac{2.899 \times 10^8}{\rho^{3/2}} \tag{38}$$

Given that

$$\delta = \frac{n_d}{fs} \tag{39}$$

the error in these are found to be

$$d\delta = \frac{1}{fs} dn_d \tag{40}$$

and

$$d\rho = -\frac{\rho^2 - R_p^2}{\rho} \frac{d\delta}{\delta} = -\frac{\rho^2 - R_p^2}{\rho} \frac{dn_d}{n_d} \tag{41}$$

The standard deviation can be approximated as

$$\sigma_\rho = \frac{\rho^2 - R_p^2}{\rho} \frac{1}{n_d} \sigma_{n_d} \tag{42}$$

10

which for $\rho >> R_p$ becomes

$$\sigma_\rho = \frac{\rho}{n_d}\sigma_{n_d} \tag{43}$$

For the LinCov Analysis, we are using $\sigma_{n_d} = 0.06 + 2.12 \times 10^{12}/\rho$ pixel so

$$\sigma_\rho = \frac{0.06\rho}{n_d} + \frac{2.12 \times 10^{12}}{\rho^{1/2}n_d} \tag{44}$$

where n_d is the expected planetary diameter in pixels.

THE VEHICLE PROCESS NOISE

Attitude Dead-banding Maneuver Errors

Given a 24-jet ESA-SM config, with attitude dead-bands with 0.028 second on-time, a recent analysis recommended a process noise of

$$Q_{Att\,Deadband} = 3.4319 \times 10^{-13} \text{ ft}^2/\text{sec}^3 \tag{45}$$

Attitude Slew Maneuver Errors

For attitude maneuvers, over a period of 3.2 hours, a Monte Carlo analysis resulted in a process noise of

$$Q_{AttSlews3.2hours} = 1.5153 \times 10^{-10} \text{ ft}^2/\text{sec}^3 \tag{46}$$

To account for varying number of slews ($= 2n_{att\,events}$) over a period of time (T_{hours}), the process noise for attitude events with a 24-jet configuration is

$$Q_{AttSlews} = 1.5153 \times 10^{-10} \left(\frac{6.4n_{att\,events}}{T_{hours}}\right) \text{ ft}^2/\text{sec}^3 \tag{47}$$

Event	Duration Between Vents (minutes)	Cycles Per Day	Process Noise $(\text{ft}^2/\text{sec}^3)$
Sleep PSA	30	16.992	1.390×10^{-9}
Awake PSA	15	45.024	2.779×10^{-9}
Active PSA	3.33	76.464	1.251×10^{-8}

Table 1. Process Noise Allocations for Astronaut Activity

PSA Puffs

For EM-2 and following, the Pressure Swing Adsorption (PSA) cycles automatically approximately every 10 minutes, less during crew sleep periods, more when the crew is awake. The PSA system can be commanded to force a complete desaturation (all vents open into space) and then they would likely not open automatically for 40-60 minutes. This would be needed during ground tracking passes and optical navigation passes.

The detailed assumptions are as follows: the maximum impulse per vent is expected to be 4.52 lbf-sec. This can be further decomposed as 0.92 lbf-sec of initial impulse and 3.60 lbf-sec of decay impulse (for a total impulse of 4.52 lbf-sec). Assuming a mass of 1650 slugs, the ΔV per vent is 2.739×10^{-3} ft/s. Assuming no preference for a particular direction, the per-axis ΔV is 1.582×10^{-3} ft/s.

Assuming that each day the astronauts will be asleep for 8.5 hours (35.4 %), awake for 11.25 hours (46.9 %) and in vigorous activity (*i.e* exercising) for 4.25 hours (17.7 %), the process noise allocations are expressed in Table 1.

The Process Noise can be calculated as

$$Q_{PSA} = 35.4\% * Q_{sleep} + 46.9\% * Q_{awake} + 17.7\% * Q_{Active} = 4.010 \times 10^{-9} \text{ ft}^2/\text{sec}^3 \quad (48)$$

The total number of vents per day is 138.48 which means that the 'average' frequency of the vents is 623.9 seconds or 10.4 minutes.

Waste Water Vents

From EM-2 onward, crewed missions will also be required to perform waste water (urine) vents. Each of these vent events have a maximum impluse (per vent) of 10.2 lbf-sec. This results in a ΔV per vent of 6.182×10^{-3} ft/sec or 3.569×10^{-3} ft/sec per axis. The resulting process noise model is described in Table 2.

Event	Duration Between Vents (hours)	Cycles Per Day	Process Noise $(\mathrm{ft}^2/\mathrm{sec}^3)$
Urine Vent	3	8	1.179×10^{-9}

Table 2. Process Noise for Waste Water Vents

Solar Radiation Pressure

A simple model presented here, based upon Wertz,[3] is

$$F_{SRP} = c_R \, p_{SR} \, A \tag{49}$$

where c_R is the coefficient of reflectivity (a value which varies between 1.0 (for perfect absorption) and 2.0 (for perfect reflectivity)), p_{SR} is a constant that contains the average/expected solar radiation pressure at 1 a.u. (in $\mathrm{N/m^2}$) and A is the expected exposed area. For Orion, the exposed area are the solar panels which are expected to be pointed toward the Sun. Therefore

$$c_R = 1.5 \tag{50}$$

$$p_{SR} = 4.51 \times 10^{-6} \ \mathrm{N/m^2} \tag{51}$$

$$A = 72.66 \ \mathrm{m^2} \tag{52}$$

$$m = 24080 \ \mathrm{kg} \ (1650 \ \mathrm{slugs}) \tag{53}$$

13

This results in

$$F_{SRP} = 1.105 \times 10^{-4} \ \mathrm{lb_F} \tag{54}$$

with the resulting acceleration

$$a_{SRP} = 6.697 \times 10^{-8} \ \mathrm{ft/s^2} \tag{55}$$

For a LINCOV integration step size of 60 seconds, the process noise is chosen to be (spreading it out in 3 axes)

$$Q_{SRP} = \left(\frac{1}{\sqrt{3}} a_{SRP} \right)^2 \Delta t = 8.970 \times 10^{-14} \ \mathrm{ft^2/s^3} \tag{56}$$

The Active Process Noise

Finally, there is the case of the ammonia sublimator running occasionally. For EM-2 and following, it is not expected that there will be any sublimator vents while in lunar orbit or close to the Moon. But the impulse prior to EI is expected to be 505.4 lbf-s for 20 minutes. The ΔV is expected to be

$$\Delta V = \frac{F \Delta t}{m} = \frac{505.4 \, \mathrm{lbf - sec}}{673 \, \mathrm{slugs}} = 0.751 \, \mathrm{ft/s} = 0.2289 \, \mathrm{m/s} \tag{57}$$

This means that

$$Q_{sublime_{CM\,only}} = \left(\frac{0.751}{\sqrt{3}} \right)^2 / 1200 \, \mathrm{sec} = 1.5667 \times 10^{-4} \ \mathrm{ft^2/sec^3} = 1.4555 \times 10^{-5} \ \mathrm{m^2/sec^3} \tag{58}$$

NAVIGATION AND DISPERSION RESULTS

The Translunar Phase

The navigation errors and trajectory dispersions for the EM-1 mission with optical navigation mapped to the B-plane are presented in Figures 3-4. For a sense of scale, these navigation errors and trajectory dispersions mapped to the B-plane with the (radius of the) Moon plotted for scale are presented in Figures 5-6.
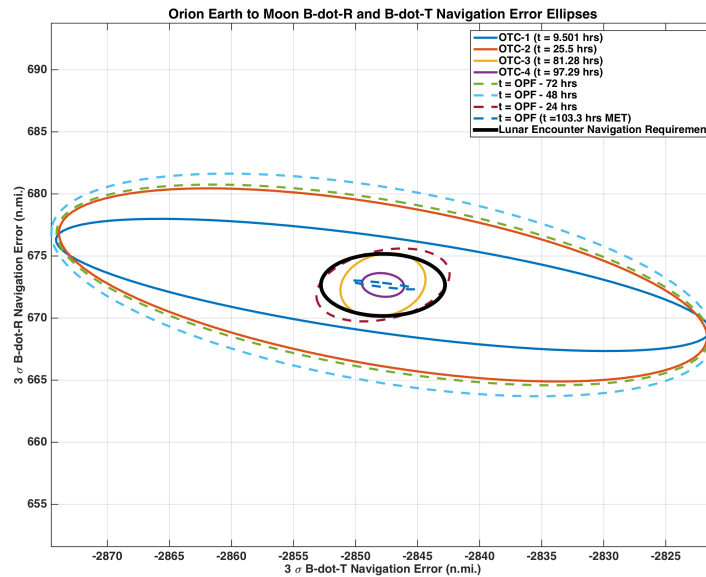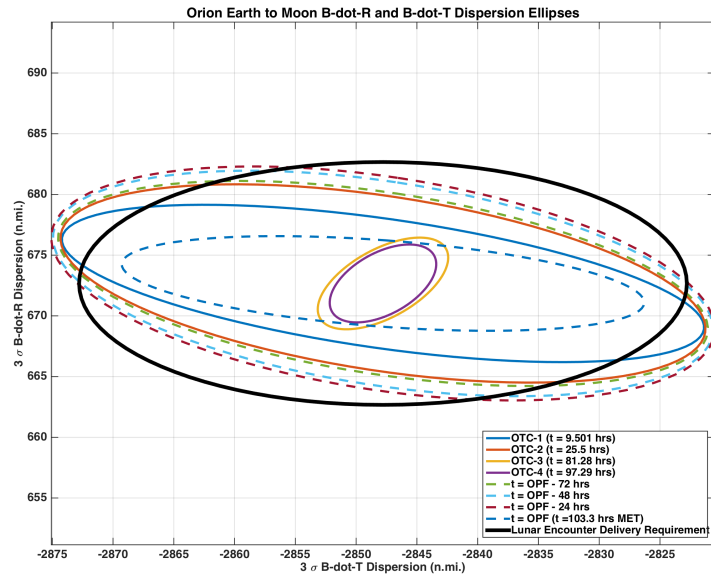

Figure 3. The Translunar Navigation Errors mapped to the B-plane (with optical navigation)

Finally, the performance at the flyby are presented in Figures 7 - 8.

Type	Lunar Flyby 3σ Value
Periapsis Altitude	0.675 n.m.
Inclination	0.0238 deg
Argument of Periapsis	0.0258 deg
C_3	$121890 \, \text{ft}^2/\text{s}^2$

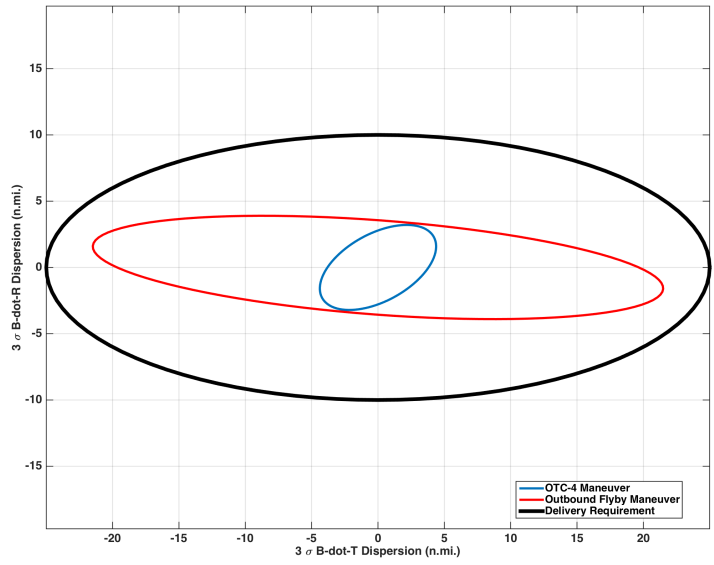**Table 3. The Trans-Lunar Delivery 3σ Statistics at OPF (with optical navigation)**

Figure 4. The Translunar Trajectory Dispersion mapped to the B-plane (with optical navigation)

Type	Lunar Flyby 3σ Value
B·T	3.90 n.m.
B·R	21.50 n.m.
Linearized Time-of-Flight	0.814 sec

Table 4. The Trans-Lunar Delivery 3σ B-plane Statistics at OPF (with optical navigation)

The TransEarth Phase

The navigation errors mapped to Entry Interface flight path angle errors are presented in Figures 9. The trajectory dispersions mapped to Entry Interface flight path angle trajectory dispersions are presented in Figures 10. Figures 11-13 contain the trajectory dispersion ellipses mapped to EI so that the correlations between the components (Downrange Position and Flight Path Angle, Velocity Magnitude and Flight Path Angle, and Crossrange Position and Crossrange Velocity) are observedThese plots also have the EI requirement displayed. One can see that that the requirement for Velocity Magnitude and Flight Path Angle is violated. The major contributor to this violation is the late ammonia sublimator vent that occurs 0.5 hour before EI.

16
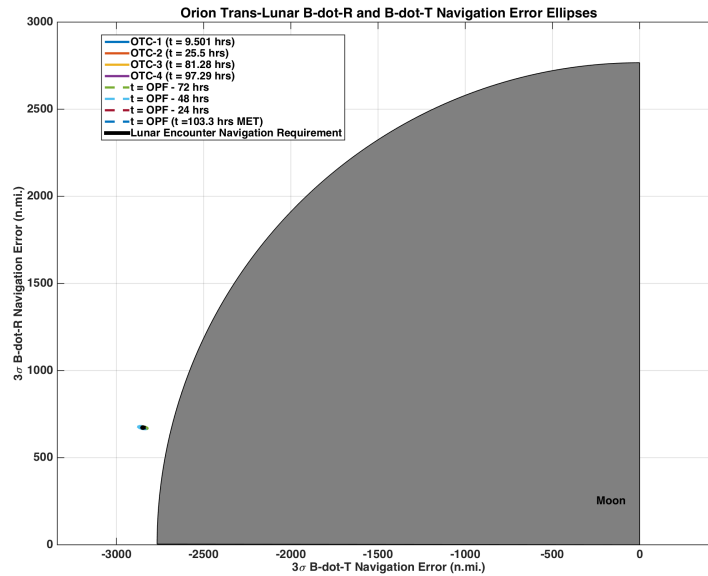
Figure 5. The Translunar Navigation Errors mapped to the B-plane (with Moon for scale) (with optical navigation)

CONCLUSIONS

This paper has described the navigation and dispersion analysis performed to date on the Orion EM-2 mission, the first crewed mission. The analysis shows that the mission meets the Entry Interface Requirements, albeit barely. The models used are conservative and will be validated on EM-1.

REFERENCES

[1] P. Maybeck, *Stochastic Models, Estimation and Control, Vol. 1*. New York, NY: Academic Press, 1979.

[2] D. K. Geller, "Linear Covariance Techniques for Orbital Rendezvous Analysis and Autonomous Onboard Mission Planning," *Journal of Guidance, Navigation and Dynamics*, Vol. 29, No. 6, 2006, pp. 1404–1414.

[3] J. Wertz, *Spacecraft Attitude Determination and Control*. Springer, 1978.
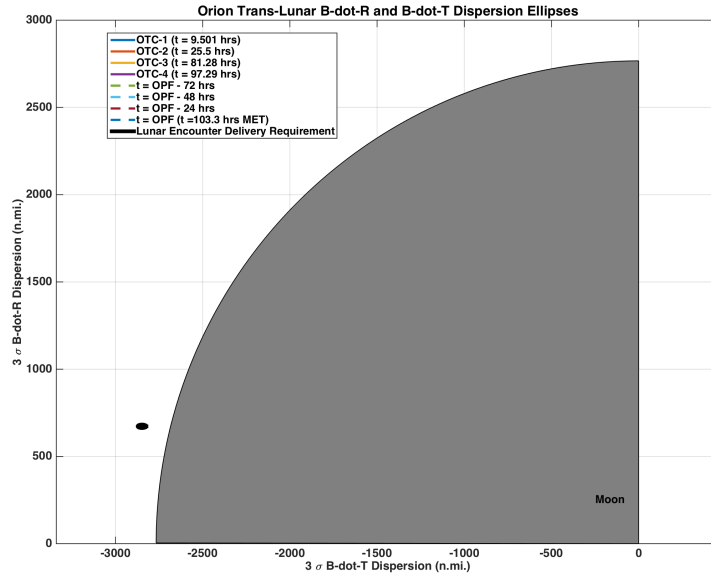
Figure 6. The Translunar Trajectory Dispersion mapped to the B-plane (with Moon for scale)(with optical navigation)
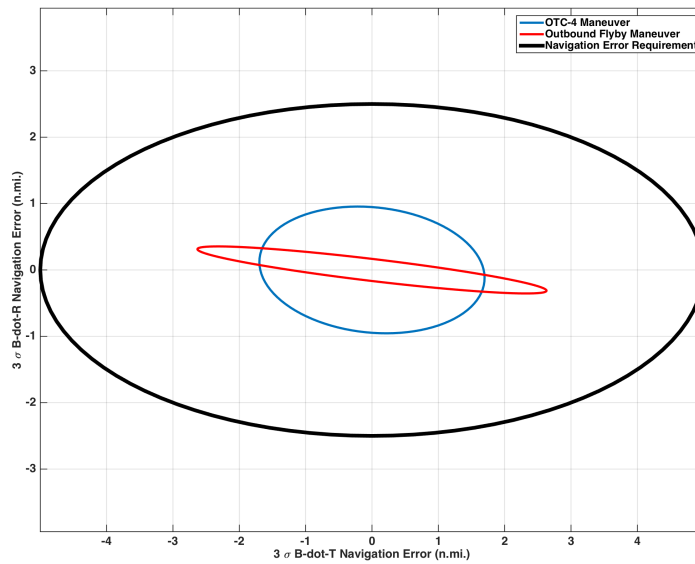
Figure 7. The Translunar Trajectory Delivery Dispersion mapped to the B-plane (with optical navigation)

Figure 8. The Translunar Trajectory Delivery Dispersion mapped to the B-plane (with optical navigation)
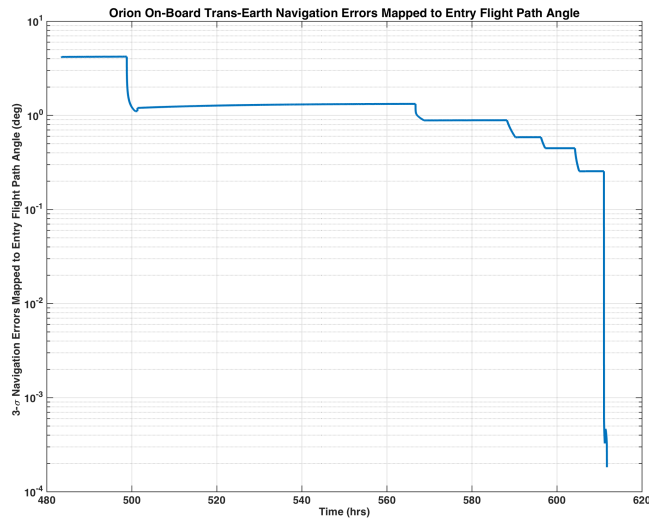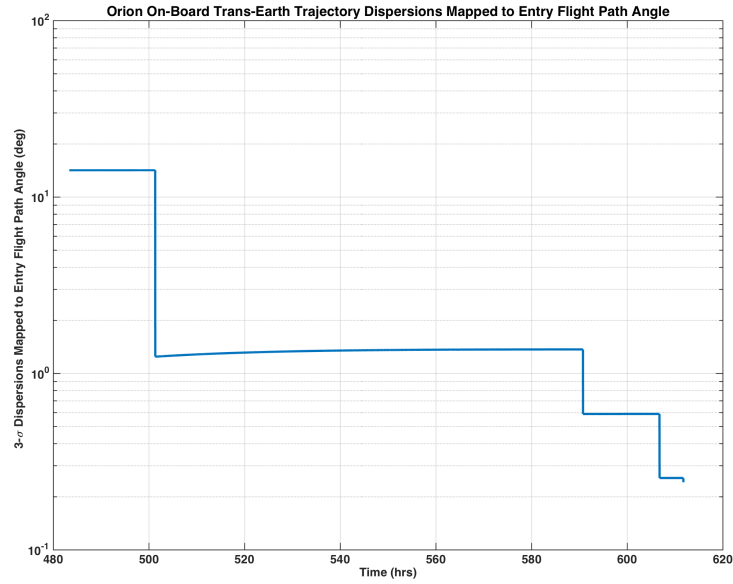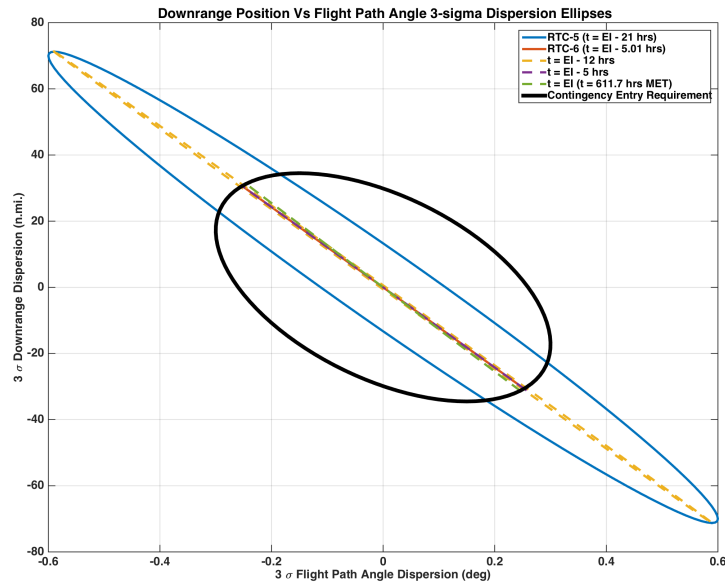

Figure 9. The on-board Navigation Errors Mapped to Entry Interface Flight Path Angle Errors

Figure 10. The Trans-Earth Trajectory Dispersions Mapped to Entry Interface Flight Path Angle Dispersions

Figure 11. The Trans-Earth Entry Interface Conditions Mapped Downrange vs Flight Path Angle Trajectory Dispersion Ellipses
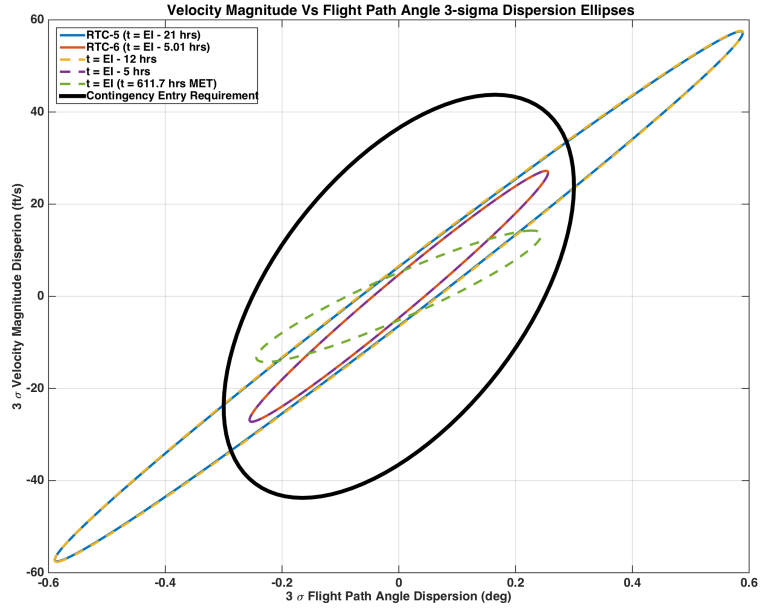
Figure 12. The Trans-Earth Entry Interface Conditions Mapped Velocity Magnitude vs Flight Path Angle Trajectory Dispersion Ellipses
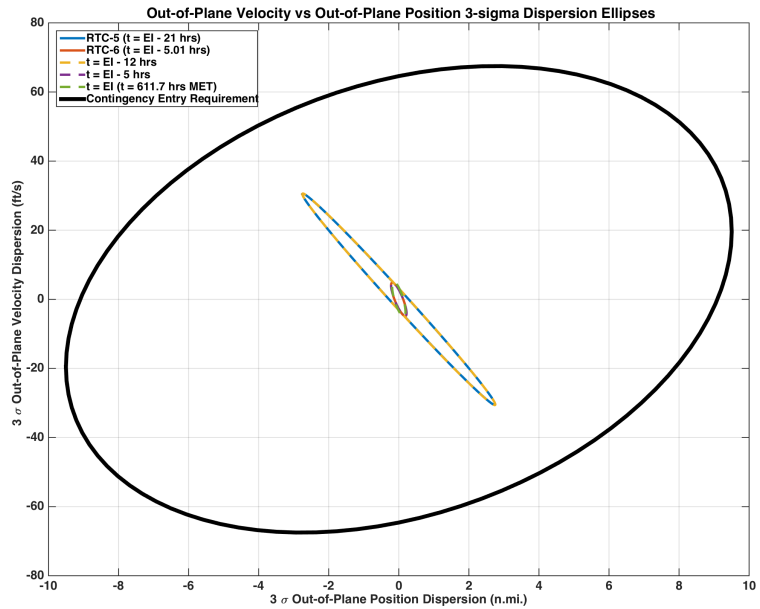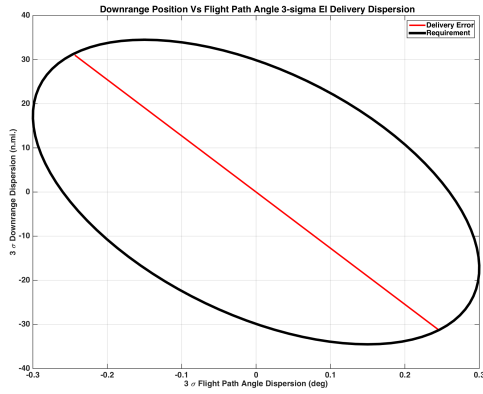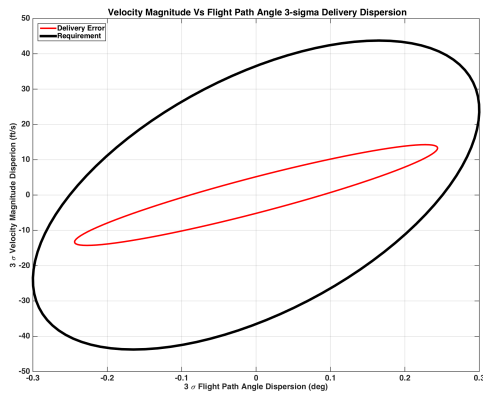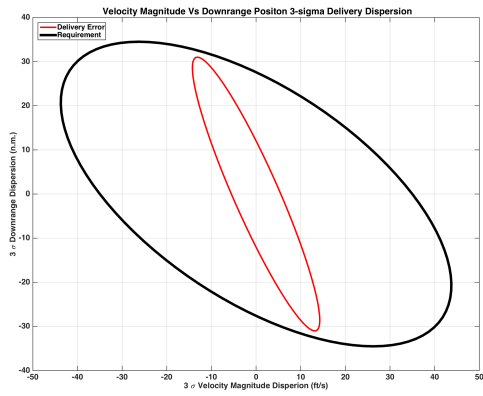

Figure 13. The Trans-Earth Entry Interface Conditions Mapped Crossrange Positon vs Crossrange Velocity Trajectory Dispersion Ellipses

Figure 14. The Trans-Earth Entry Interface Conditions Mapped Downrange vs Flight Path Angle Delivery Error Ellipses

Figure 15. The Trans-Earth Entry Interface Conditions Mapped Velocity Magnitude vs Flight Path Angle Delivery Error Ellipses

22

Figure 16. The Trans-Earth Entry Interface Conditions Mapped Velocity Magnitude vs Downrange Delivery Error Ellipses

Figure 17. The Trans-Earth Entry Interface Conditions Mapped Crossrange Positon vs Crossrange Velocity Delivery Error Ellipses